




Future projection of heat waves over China under global warming within the CORDEX-EA-II project

Pinya Wang^{1,2} · Pinhong Hui³ · Daokai Xue² · Jianping Tang^{1,2} 

Received: 4 August 2018 / Accepted: 8 January 2019 / Published online: 14 January 2019
© Springer-Verlag GmbH Germany, part of Springer Nature 2019

Abstract

Driven by four global climate models (GCMs) from the Coupled Model Intercomparison Project Phase 5 (CMIP5) (i.e., CNRM-CM5, EC-EARTH, GFDL-ESM2M and MPI-ESM-LR) under the Representative Concentration Pathway 8.5 (RCP8.5) scenario, projections for future changes in heat waves over China are performed by Weather Research Forecasting (WRF) model simulations for future (FTR, 2031–2055) and present (1981–2005) periods. Six heat wave indices are applied to characterize heat waves based on their frequency, duration, magnitude, intensity, accumulated occurrence days and severity. Analyses show that notable increases in heat wave indices cover all of China. More areas will endure more frequent, longer lasting and more severe heat waves in the coming decades. The increasing tendencies of heat wave indices in the FTR period are more significant than those at present, indicating that heat waves will intensify more rapidly in the future. The impacts of climate changes on the accumulated properties of heat waves are more substantial than those on the individual aspects of heat waves. It is also projected that stronger heat waves with prolonged durations and more severe magnitudes will occur more often in the FTR period, whereas relatively weaker heat waves would occur less often. Hence, the occurrence of extreme heat waves shows a more remarkable increase than the occurrence of moderate heat waves. The changes in heat waves can be largely explained by the changes in the dominating high-pressure systems.

Keywords Heat waves · WRF · CORDEX-EA-II · Future projection

1 Introduction

Global warming is an unequivocal fact, and many of the observed changes in climate systems are unprecedented over decades to millennia. The atmosphere and ocean have warmed, the amounts of snow and ice have diminished, and sea level has risen. The globally averaged combined land and ocean surface temperature, as calculated by linear trend, shows a warming of 0.85 °C over the period 1880

to 2012 (IPCC 2014). The global mean surface temperature is expected to continue to rise by 1.4–5.8 °C over the period from 1990 to 2100 due to the projected increases in greenhouse gas concentrations in the atmosphere (Boo et al. 2006).

The warming climate is likely to cause changes in the characteristics of extreme weather events, as noted by, e.g., Meehl et al. (2000), Griffiths et al. (2005), Tebaldi et al. (2006), Russo and Sterl (2011), Orłowsky and Seneviratne (2011), and Sillmann et al. (2013). For example, under global warming scenarios, heat waves, usually defined as the extreme temperatures above a threshold near the upper ends of the observed values, are expected to be more frequent, intense and/or longer lasting (Meehl and Tebaldi 2004; Cowan et al. 2014; Dosio 2016). Associated with these changes are higher risks of disastrous consequences for human, natural and industrial systems. Prolonged periods of extremely high temperatures and a dry atmosphere could lead to an increase in the frequency and severity of forest fire, tree mortality, agricultural loss, overburden electricity and water facilities (Barriopedro et al. 2011; Field et al.

Electronic supplementary material The online version of this article (<https://doi.org/10.1007/s00382-019-04621-7>) contains supplementary material, which is available to authorized users.

✉ Jianping Tang
jptang@nju.edu.cn

¹ Key Laboratory of Mesoscale Severe Weather/Ministry of Education, Nanjing University, Nanjing 210023, China

² School of Atmospheric Sciences, Nanjing University, 163 Xianlin Road, Nanjing, China

³ Jiangsu Climate Center, Nanjing 210009, China

2012; Unal et al. 2013). Moreover, more intense heat waves would cause increased morbidity and mortality (Perkins 2015). Therefore, understanding the potential future changes in heat waves has important implications for human and ecosystem acclimation. In addition, it is of considerable importance for policymakers to advance climate change adaptations by evaluating the future risks and impacts caused by changes in extreme temperatures (IPCC 2014). Many studies have investigated the future projections of heat waves at global and regional scales. Beniston et al. (2007) presented an overview of changes in the extreme events over Europe and found that regional surface warming could cause the frequency, intensity and duration of heat waves to increase. In addition, the intensity of extreme temperatures increases more rapidly than the intensity of more moderate temperatures over the continental interior due to increases in temperature variability. Boo et al. (2006) investigated the possible changes in extreme temperatures over Korea in the coming century and reported that hot events are expected to be more frequent and intense under the current climate change scenario. With an ensemble of regional climate model (RCM) simulations, it is suggested that there is a high probability of heat waves of unprecedented severity over the continental US by the end of the twenty-first century if a high emissions path is followed (Kunkel et al. 2010). Based on the results of a very high-resolution global model, Dosio et al. (2018) demonstrated that heat wave magnitude is expected to increase over Africa, South America, and Southeast Asia. Compared to a world with an increase of 1.5 °C in global average surface temperature, the frequency of extreme heat waves would double across most of the globe under with 2.0 °C warming.

The projected changes in heat waves have also become a great concern for China. Guo et al. (2016) investigated the projection of heat waves over China using 12 Coupled Model Intercomparison Project Phase 5 (CMIP5) models, and the results showed that the frequency and intensity of heat waves would increase more dramatically as the increase in the global mean temperature attained higher warming targets. Under the Representative Concentration Pathway 4.5 (RCP4.5) scenario, by the middle of the twenty-first century, the heat wave duration index over China is expected to be multiplied 2.6 times longer based on a multi CMIP5 model ensemble (Yao and Luo 2012). Based on the output of 17 CMIP5 models, Zhang (2012) analyzed the spatiotemporal features of 2.0 °C warming of surface temperatures over the globe and in China under the RCP4.5 scenario and found that surface warming over China occurs substantially faster than the global mean. Most of the previous studies are based on the multiple CMIP5 models (Taylor et al. 2012), which are global climate models (GCMs). With a coarse resolution, GCMs are limited with respect to some processes that are influenced by e.g. topographical details, coastlines, and

land-surface heterogeneities (Dosio 2016). Regional climate models (RCMs) generally show improved skill at capturing such detailed processes and have been widely used for simulating extreme events (e.g. Fischer et al. 2007; Lhotka and Kyselý 2015; Wang et al. 2018). Yang et al. (2010) investigated the projected change in heat waves over China from one run of a regional model (PRECIS) using the IPCC Special Report on Emissions Scenario A2. Ji and Kang evaluated several kinds of extreme weather events over China projected for the end of the twenty-first century (2080–2099) with the regional climate model RegCM4. The Coordinated Regional Climate Downscaling Experiment (CORDEX, <http://wcrp-cordex.ipsl.jussieu.fr>) was implemented under the auspices of the World Climate Research Program (WCRP). The CORDEX aims to advance and coordinate the science and application of regional climate downscaling through global partnerships (Giorgi et al. 2009; Giorgi and Gutowski 2015). With the development of the RCMs and the demand for higher resolution, the CORDEX is now underway to improve the experimental framework leading to its second phase (CORDEX-II). With a domain focused on East Asia (<https://cordex-ea.climate.go.kr/main/modelsPage.do>), the second phase of CORDEX-East Asia (CORDEX-EA-II) will use the new domain with 0.22°, or 25 km, resolution (Zhou et al. 2016).

Considering the two predominant challenges that China will experience in the coming decades (i.e., the increased aging population and the continued urbanization), a more vulnerable Chinese population is about to be exposed to the threat of extreme heat. Lu and Chen (2016) call for more attention paid to the temperature extremes, particularly on high temperature extremes under global warming. Thus, in this study, over the CORDEX-EA-II frame, the RCM Weather Research and Forecasting (WRF) model is utilized to investigate the future changes in heat waves over China under the global warming scenario. Considering the various local climate conditions over China, heat waves are identified by a percentile-based definition and several heat wave indices are applied to quantify heat waves' properties. Section 2 introduces the data, methods, and experimental design. The Results and analyses are presented in Sect. 3. Summary remarks are presented in the Sect. 4.

2 Data, method and experimental design

2.1 Model and experimental design

In this study, the WRF model (version 3.6.1, Skamarock et al. 2008) is used to downscale the results of four GCMs from the CMIP5: CNRM-CM5, EC-EARTH, GFDL-ESM2M and MPI-ESM-LR. The WRF model has been widely used for regional simulations of extreme temperatures

over East Asia and shows good performance (Tang et al. 2016; Wang et al. 2018). The initial and boundary conditions in the WRF simulations are provided by the four CMIP5 GCMs, which all show good performance in simulating the regional climate of East Asia (Chen and Sun 2013; Bosmans et al. 2018). Following the CORDEX-EA-II framework, the simulation domain covers all of China and East Asia (Fig. 1) at a resolution of 25 km. The historical runs (1981–2005) for present climate are forced by the natural and anthropogenic atmospheric composition and defined as the reference (RF) experiments, whereas the future projections (2031–2055) are forced by the warming scenario Representative Concentration Pathways 8.5 (RCP8.5) and defined as the future (FTR) experiments. The simulation periods are from 1979 to 2005 for the RF experiments and from 2029 to 2055 for the FTR experiments, of which the first 2 years are used as the spin-up time in all the experiments.

The experimental physics options used in this study are the same as those in the CORDEX-EA-I experiments (Tang et al. 2016; Wang et al. 2018), including the microphysics scheme of the WRF Single-Moment 5-class (WSM5) (Lim and Hong 2010), the convective parameterization scheme based on Kain and Fritsch (1990), the Yonsei University planetary boundary layer scheme (YSU PBL) (Hong et al. 2006) and the NOAA land surface scheme (Chen and Dudhia 2001).

2.2 Heat wave definition and validation data

In the present study, a heat wave is defined the same as that in Wang et al. (2017b, 2018). A heat wave occurs when the daily maximum temperature exceeds the temperature threshold for at least 4 consecutive days. For each calendar day during May–September, the temperature threshold is calculated as the 90th percentile of a 21-day-long moving-center window

(following Stefanon et al. 2012) over the reference period (1981–2005). Likewise, we quantify heat waves based on the six heat wave indices defined and used in Wang et al. (2017b, 2018), i.e., the number of heat waves in a given period (HWN), mean heat wave duration (HWDU), mean heat wave magnitude (HWM), mean heat wave intensity (HWI), total heat wave duration (HWF) and total heat wave intensity (HWTI). Among them, HWN, HWDU and HWM are single-aspect indices that characterize three distinct aspects of heat waves, whereas HWI, HWF and HWTI are integrative indices, which merge several aspects into one single value. Furthermore, the HWDU, HWM and HWI describe the characteristics of individual heat wave events (i.e., their mean duration, magnitude and intensity), whereas the HWN, HWF and HWTI characterize the accumulated properties of all heat wave events over a period of time.

As in Wang et al. (2017b, 2018), for heat waves over a specific period (e.g. 1 year or the whole research period), the six heat wave indices are defined as follows:

$$HWN = N \tag{1}$$

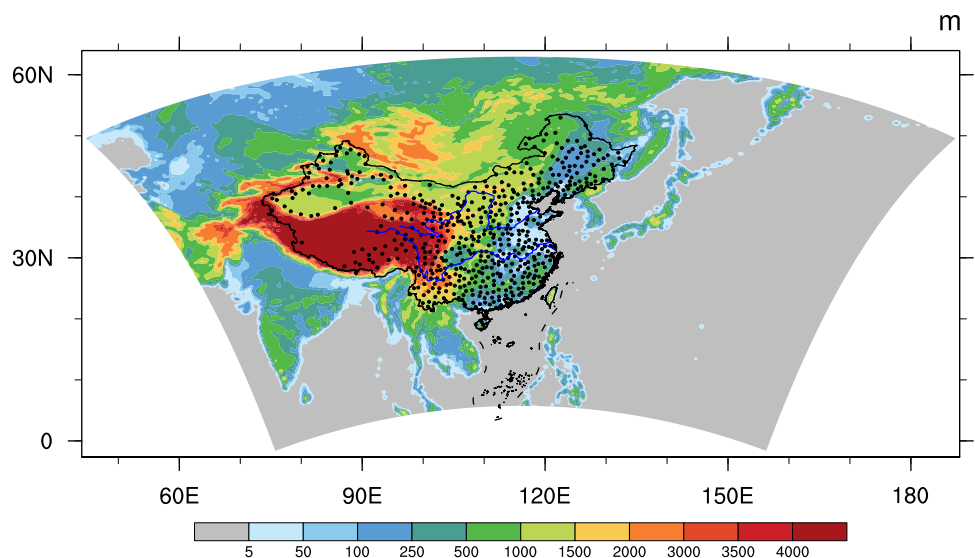
$$HWDU = \frac{\sum_{i=1}^N (D_i)}{N} \tag{2}$$

$$HWM = \frac{\sum_{i=1}^N \frac{\sum_j^{D_i} (T_{ij} - TR_{ij})}{D_i}}{N} \tag{3}$$

$$HWI = \frac{\sum_i \sum_j^{D_i} (T_{ij} - TR_{ij})}{N} \tag{4}$$

$$HWF = \sum_i D_i = HWDU \times HWN \tag{5}$$

Fig. 1 The topography (color shading) over the simulation domain (grey shading), and the 587 observation sites (black dots)



$$\text{HWTI} = \sum_i^N \sum_j^{D_i} (T_{ij} - \text{TR}_{ij}) = \text{HWI} \times \text{HWF} \quad (6)$$

where N is the total number of heat wave events for this period; for the heat wave i , its intensity, $\sum_j^{D_i} (T_{ij} - \text{TR}_{ij})$, is calculated as the sum of the temperature deviation exceeding the threshold throughout its duration D_i . T_{ij} and TR_{ij} are the T_{max} and the corresponding threshold for day j during this heatwave.

To evaluate the model performance on simulating observed heat wave events, daily maximum temperatures over the period of 1981–2005 from 587 observational sites across China are used (black dots in Fig. 1). This dataset is provided by the National Meteorological Information Center of the China Meteorological Administration (CMA), which has been quality controlled and homogenized (Li et al. 2004). The dataset has been widely used for research on extreme weather events in China (e.g., Ding et al. 2010; Wang et al. 2015, 2018). For convenience of comparison, the results of WRF simulations are interpolated to the observational sites using bilinear interpolation method. Geopotential heights at the 500 hPa level (H500), derived from the new Japanese 55-year Reanalysis by the Japan Meteorological Agency (JRA-55, Ebata et al. 2011) is used to validate the ability of WRF to simulating the atmospheric circulations during heat waves.

3 Results

3.1 Evaluation of heat wave simulations under present climate condition

In this section, we first evaluate the ability of the WRF model to reproduce the observed heat waves under present climate condition through the comparison between the observed and simulated heat wave indices, and then depict the overall capacity of the model to simulate the spatial variability of the observed heat waves by the Taylor diagram (Taylor 2001).

Figure 2 shows the spatial patterns of the singular heat wave indices in the observation and the WRF simulations during the RF period (1981–2005). For HWN, high values in the observation are mainly located at southeastern China and Xinjiang province (Fig. 2a), which is consistent with previous results from Wang et al. (2018). In WRF simulations, the CNRM-CM5 and EC-EARTH driven runs can reasonably reproduce the HWN values over Xinjiang while they underestimate the HWN values over southeastern China and the middle reaches of the Yellow River (Fig. 2c, d). The GFDL-ESM2M and MPI-ESM-LR driven runs appear to better capture the spatial features of HWN with reasonable

values over most of China (Fig. 2e, f). However, all the four GCM-driven runs overestimate the HWN values over the eastern Tibetan Plateau. Consequently, the ensemble of four WRF simulations is able to reproduce the spatial patterns of HWN values reasonably well, though with overestimation over the eastern Tibetan Plateau and some underestimation over southeastern China (Fig. 2b). The observed HWDU shows relatively higher values along the Yellow River and in southeastern China (Fig. 2g). The CNRM-CM5 and EC-EARTH driven runs exhibit similar patterns of HWDU, overestimating it over northwestern China but underestimating it over northeastern China (Fig. 2i, j). Likewise, the GFDL-ESM2M and MPI-ESM-LR driven runs show underestimated HWDU values over northeastern China and overestimated HWDU over northwestern China. In addition, they produce greater HWDU values than the observations in southeastern China (Fig. 2k, l), especially in the MPI-ESM-LR driven run (Fig. 2l). Accordingly, the ensemble of four model simulations can generally capture the spatial distributions of HWDU values but overestimates it over southeastern and northwestern China and shows underestimation in northeastern China (Fig. 2h). For the observed HWM, there is a progressive increase from the south to the north of China (Fig. 2m). This phenomenon has been revealed in previous studies and is caused by the more severe warming over the northern China in recent decades (e.g., Wang et al. 2017a). The four GCM-driven runs show great consistency in simulating the spatial distributions of HWM values and exhibit a positive gradient of HWM values from south to north China (Fig. 2o–r). Among the four experiments, the CNRM-CM5 and EC-EARTH driven runs seem to perform better for simulating the HWM values (Fig. 2o, p), while the GFDL-ESM2M and MPI-ESM-RL driven runs tend to overestimate HWM values over the northern part of China (Fig. 2q, r). Consequently, the ensemble results of four model simulations show a reasonable representation for the spatial distributions of HWM but overestimate its magnitude over the northern part of China (Fig. 2n).

In addition to the single-aspect heat wave indices, the evaluation is also performed on the integrative indices (Fig. 3). For the HWI, which merges the properties of HWDU and HWM, higher values are observed over northern China (Fig. 3a), which is consistent with previous results that heat waves in northern China are more severe than those in southern China, as noted by Wang et al. (2017a). The four GCM-driven runs can reasonably reproduce the spatial patterns of HWI values (Fig. 3c–f). However, biases exist in the simulations, especially in the GFDL-ESM2M and MPI-ESM-LR driven runs (Fig. 3e, f). These WRF simulations tend to overestimate the HWI values over the middle and lower reaches of Yangtze River, as well as the north part of China, with larger biases in the MPI-ESM-LR driven simulation (Fig. 3f). Their ensemble characterizes the

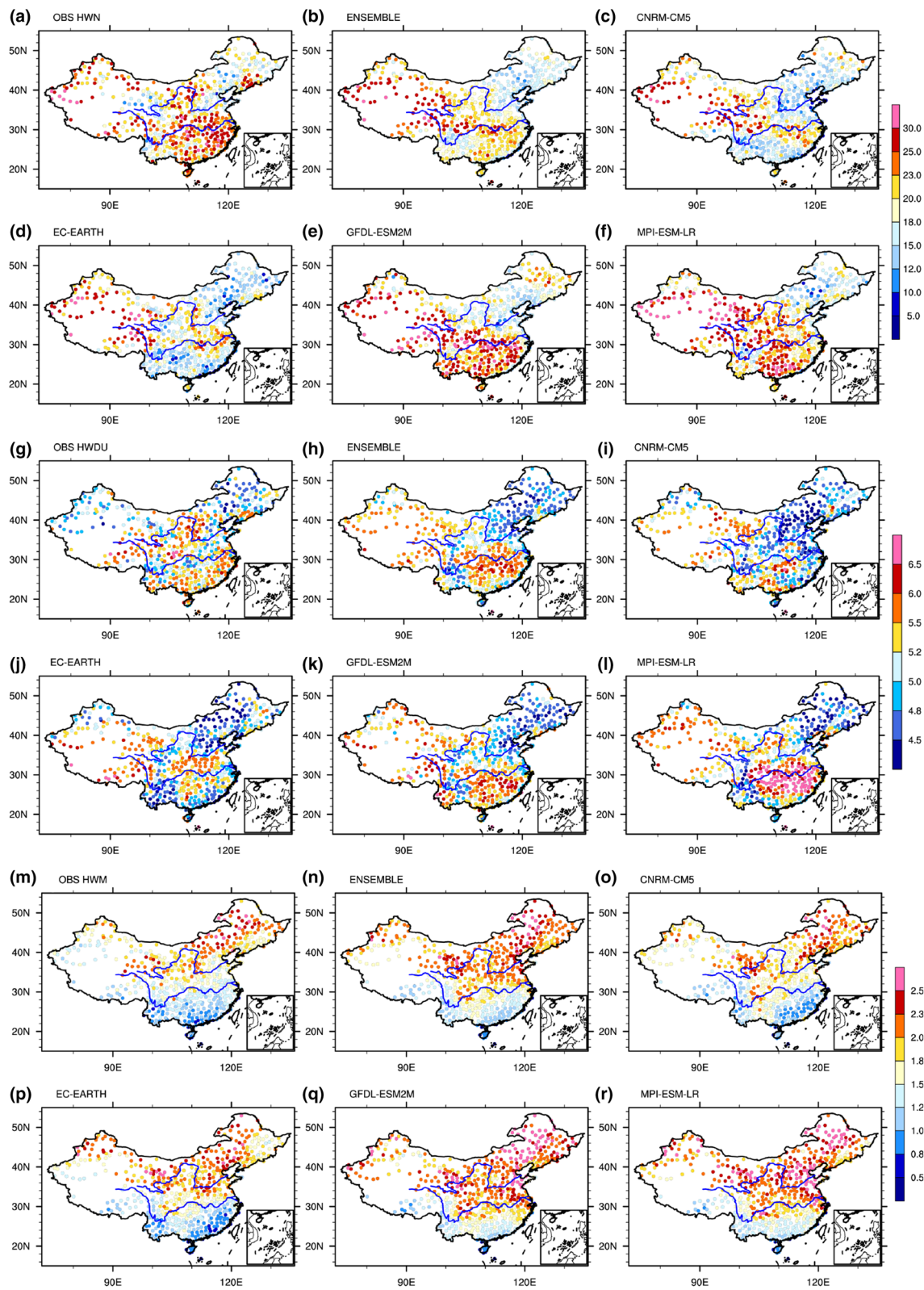


Fig. 2 The spatial distributions of observed (a) and simulated HWN (unit: events) in WRF runs driven by CNRM-CM5 (c), EC-EARTH (d), GFDL-ESM2M (e) and MPI-ESM-LR (f) and the model ensemble

(b). **g-l** and **m-r** are same as (a-f), but for HWDU (unit: days/event) and HWM (unit: °C/day)

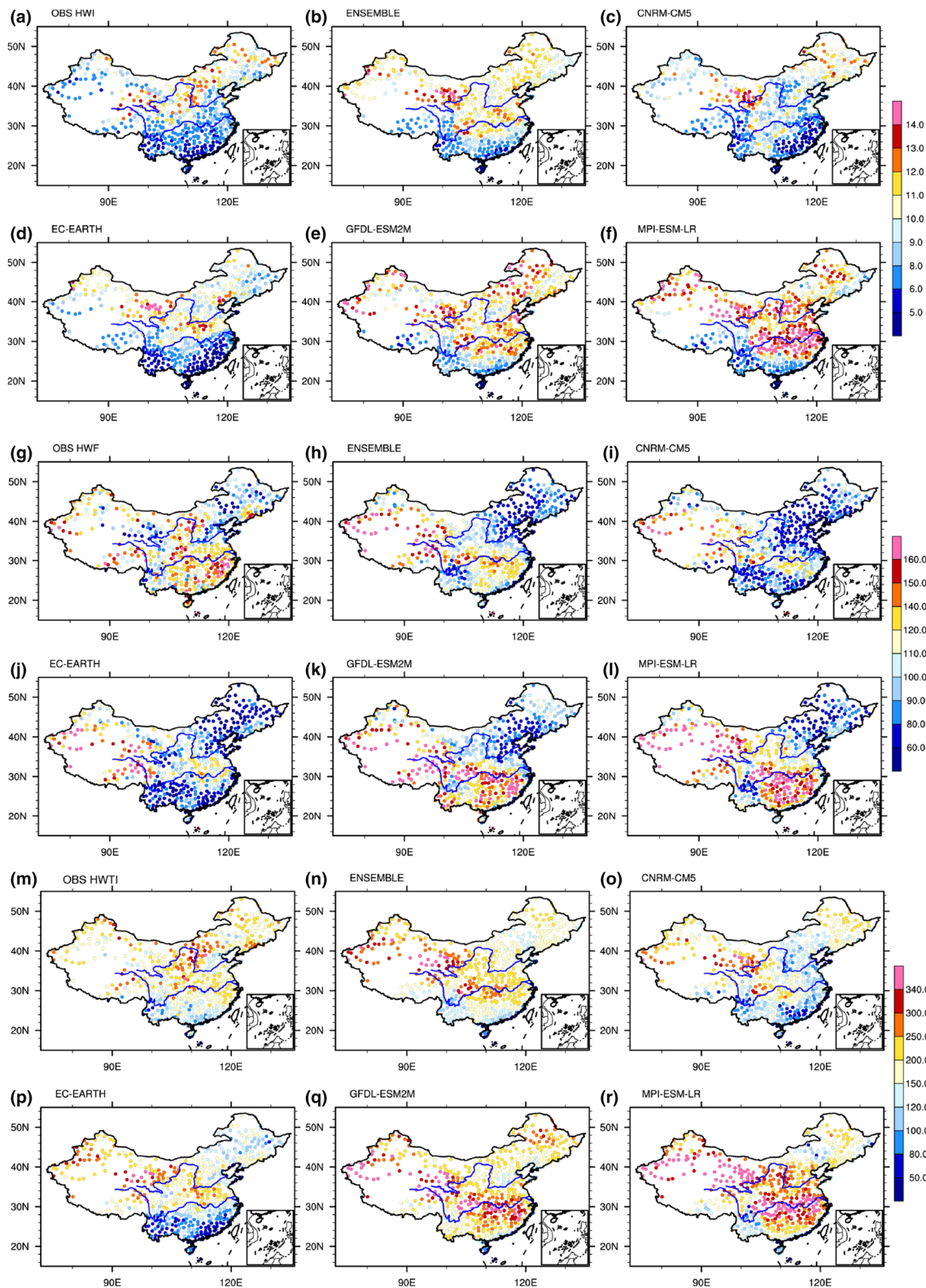


Fig. 3 Same as in Fig. 2, but for HWI (a–f, unit: °C/event), HWF (g–l, unit: days) and HWTI (m–r, unit: °C)

spatial distributions of HWI reasonably well but somewhat overestimates its values over the middle and lower reaches of the Yangtze River and northwestern China (Fig. 3b). As the combination of HWN and HWDU, the observed HWF values are higher over southeastern and northwestern China, and lower over northeastern China (Fig. 3g). The WRF model simulations driven by CNRM-CM5 and EC-EARTH can reasonably reproduce the spatial patterns of HWF but overestimate HWF values over the eastern Tibetan Plateau and underestimate its values over the southern and northeastern areas in China (Fig. 3i, j). The GFDL-ESM2M and MPI-ESM-LR driven runs can reasonably demonstrate the spatial patterns of HWF, while overproduce the values in the areas with high HWF and underestimate them in low-HWF areas (Fig. 3k, l). The ensemble can reasonably reproduce the spatial distribution of HWF but overestimates its values over northwestern China and produces lower HWF values over the northeastern areas in China (Fig. 3h). The integrative index HWTI is the combination of HWI and HWN and shows higher values over the northern regions of China in the observations (Fig. 3m). The four GCM-driven runs can reasonably reproduce the spatial features of HWTI, although biases exist in the simulations of HWTI values (Fig. 3o–r). The four WRF simulations tend to overestimate the HWTI values over northwestern China (Fig. 3o–r). In addition, the GFDL-ESM2M and MPI-ESM-LR driven runs obviously overestimate the HWTI values over southern part of China (Fig. 3p–r). Accordingly, the ensemble results of the four WRF simulations show a reasonable representation of the

spatial features of the HWTI values, whereas the HWTI values over northwestern China are overestimated (Fig. 3n).

The Taylor diagram is used to quantitatively evaluate the ability of the WRF model to simulate the spatial variability of the heat wave indices (Fig. 4). The radial coordinate gives the standard deviation of the model results divided by the standard deviation of the observed values, which compares the magnitude of spatial variability of the heat wave indices. The angular coordinate is the correlation coefficient between the model results and the observation. For the singular indices (i.e., HWN, HWDU and HWM, Fig. 4a), the WRF model simulations show a greater ability to reproduce the HWM with correlations higher than 0.75. The performance of the WRF model in reproducing the spatial variability of HWN and HWDU varies depending on the driving GCMs, with correlations ranging from 0.2 to 0.5. Moreover, for each of the three singular-aspect heat wave indices, the ensemble result of the four GCM-driven runs shows improved skill in reproducing the spatial variability, with higher correlation with the observation, and a standardized deviation closer to the observation. For the three integrative indices (HWI, HWF and HWTI, Fig. 4b), the four GCM-driven runs can reasonably reproduce their spatial features with correlations between 0.3 and 0.7, although the simulations tend to overestimate their spatial variability. Consistent with the results for the singular heat wave indices, the model ensemble shows better representations of the spatial variability in the integrative heat wave indices than the individual simulations among the four GCM-driven runs, with higher correlations

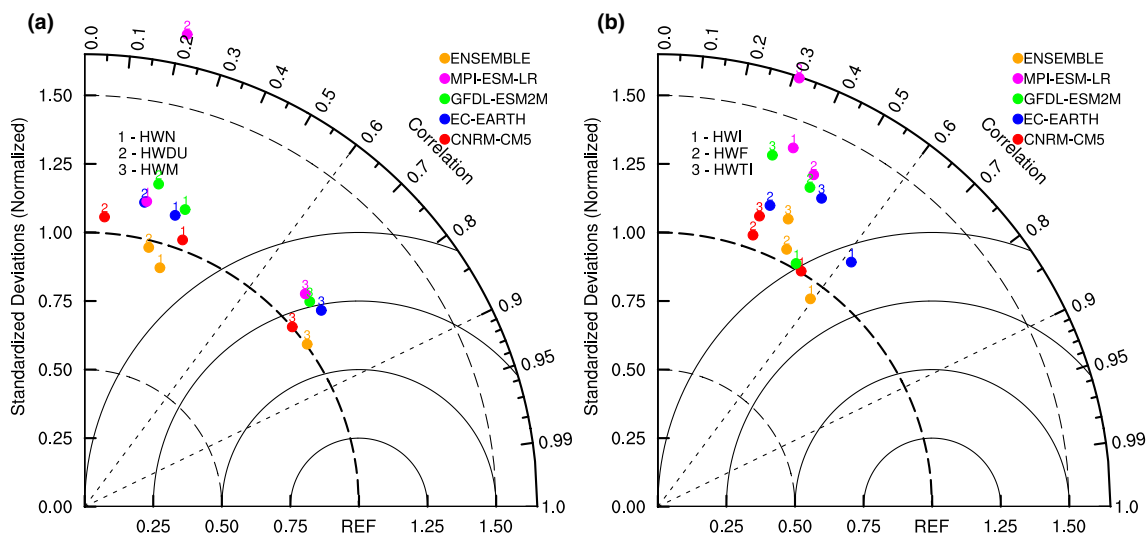


Fig. 4 Taylor diagram for the spatial variabilities of **a** singular (i.e., HWN, HWDU and HWM) and **b** integrative (i.e., HWI, HWF, and HWTI) heat wave indices in WRF runs driven by different GCMs. The radial distance from the original point represents the ratio between the observed and simulated spatial standard deviations for

averaged heat wave indices during 1981–2005. The azimuthal position gives the spatial correlation coefficient between the observed and simulated heat wave indices. The distance from the REF point demonstrates the normalized centered root mean square error (RMSE)

with the observations and better representation of the standard deviations.

The evaluation of the model results for the present climate is performed not only for the RCMs, but also for the corresponding driving GCMs. The WRF model is not always able to improve the performances of all the four driving GCMs. However, added value is gained in simulating the spatial variability in WRF simulations compared to most of the driving GCMs, and in simulating the temporal variability driven by GFDL-ESM2M and MPI-ESMLR. In particular, the inter-model spread of results produced by GCMs is reduced in the WRF simulations (see the discussion of Fig. S4–S8 in the supplementary material). Dosio et al. (2015) evaluated the downscaling of CMIP5 GCMs (MPI-ESM-LR, HadG2M2-ES, CNRM-CM5 and EC-EARTH) over CORDEX-Africa with COSMO-CLM and similar results were found.

3.2 Synoptic circulation during heat waves

The anomalous high-pressure system is a common feature to sustain most heat wave events (Matsueda 2011; Pezza et al. 2012). To assess the ability of the WRF model to reproduce the synoptic circulation dominating heat wave events, the H500 anomalies during heat waves derived from reanalysis data are compared to those produced by the WRF model. Following Zittis et al. (2016), the synoptic circulation during heat waves are analyzed based on three sites at different locations. According to Zittis et al. (2016), anticyclones that sustain heat waves can have a radius of more than 1,000 km; hence, the three sites located at eastern (45°N, 123°E), northwestern (42°N, 85°E) and southeastern China (25°N, 115°E) are approximately representative of the domain of China. We created the maps of H500 anomalies averaged for heat wave occurrence days over the three selected sites during the reference period (1981–2005) for the observed and the simulated heat waves in the four WRF simulations. The H500 anomalies are obtained by removing the average of H500 from May to September during 1981–2005. For the observed heat waves, the H500 data from the JRA55 reanalysis is used, whereas the simulated heat waves use the H500 produced by the four GCM-driven WRF runs.

The average H500 anomalies in the observations and the ensemble of four WRF simulations are shown in Fig. 5. It has been demonstrated that each of the three sites is dominated by anomalous high-pressure systems when heat waves occur (Fig. 5a, c, e). The spatial pattern and magnitude of the H500 anomalies can be generally captured by the ensemble of WRF simulations (Fig. 5b, d, f), and the WRF model is able to correctly locate the high value centers of the H500 anomalies. According to the observations and our simulations (Fig. 5a–d), heat waves at the sites over northeastern and northwestern China are controlled by the center of H500 anomalies directly overhead. Such structures are usually

known as blocking high and were positioned in the same region for a longer period than expected (Perkins 2015). Under the control of blocking highs, warm air over the mid-high latitudes cannot mix with cold air and builds up, thus causing warm weather events, such as the great 2010 heat wave in Russia. Moreover, adiabatic heating due to subsidence over the center of blocking highs is also important for heat wave generation (Matsueda 2011). For the site in southeastern China (Fig. 5e, f), the circulation pattern is similar, although the center of the high-pressure system is more to the eastward of heat waves. Such anomalous high-pressure systems are usually associated with Rossby wave propagations and are responsible for numerous heat waves at lower latitudes (Hudson et al. 2011; Pezza et al. 2012). It should be noted that such anomalous high-pressure patterns for heat waves in different regions are produced by each of the four WRF simulations (see Fig. S1–S3 in supplementary material).

3.3 Future changes in heat waves

The following analyses investigate the future changes in heat wave characteristics by comparing heat wave indices over the RF (1981–2005) and the FTR (2031–2055) periods. The first subsection focuses on the changes in the climatological features of heat waves, whereas the second subsection concentrates on the changes in the characteristics of individual heat wave events.

3.3.1 Future changes in the climatological heat wave indices

Figure 6 illustrates the spatial distributions of future changes in heat wave indices projected by the model ensemble between future projection (2031–2055) and current climate (1981–2005). It should be noted that the changes in heat waves herein cover the period of 25 years. To assess the robustness of the projected heat wave changes, both the absolute changes (FTR-RF) and the ratios of changes to the intermodel spread are shown. The intermodel spread is defined as the standard deviation among the results in the four WRF simulations. A ratio > 1.0 indicates a robust ensemble result, while a ratio ≤ 1.0 means that relatively high uncertainty exists among the multi-model simulations; thus, the result of the model ensemble cannot be qualified as robust (Li and Zhou 2010).

For HWN, positive changes cover all of China with greatest increase over 70 events in southern China and in part of the Tibetan Plateau, while the changes are weaker over northeastern China (Fig. 6a). The corresponding ratios to the intermodel spread are higher than 3.0 over the whole domain of China, with the maximum exceeding 10.0 in the northern part of China. These results indicate the robustness of the

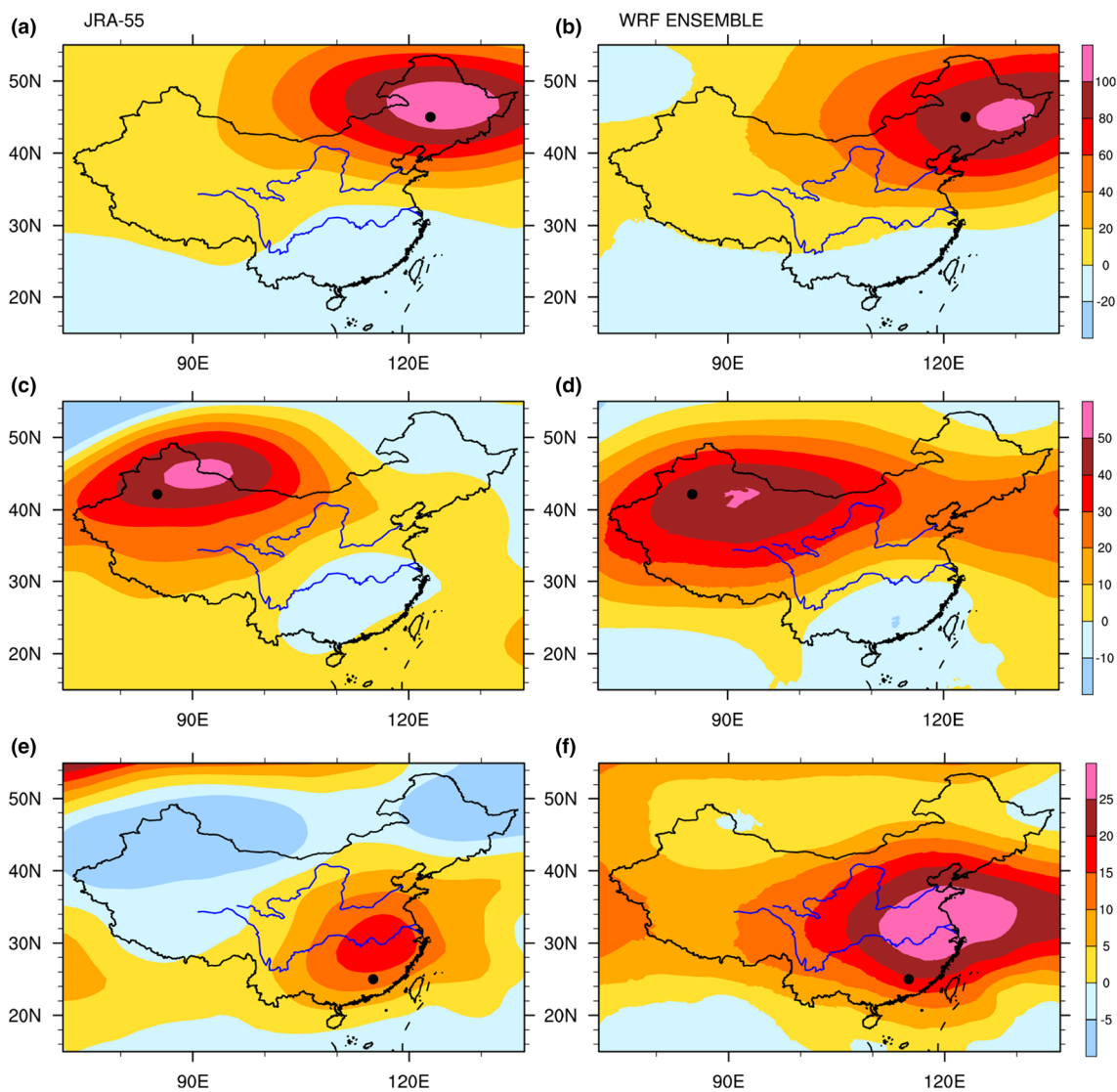


Fig. 5 The H500 anomalies (unit: m) during heat wave occurrences at eastern (45°N, 123°E), northwestern (42°N, 85°E) and southeastern China (25°N, 115°E) from the JRA55 reanalysis (a, c, e) and the ensemble of the four GCM-driven WRF runs (b, d, f)

projected changes in the model ensemble, and especially higher over the northern China. The changes in HWDU exhibit a similar spatial pattern to those of HWN, with maximum increase over 1 day/event occurring over southern China, part of the Tibetan Plateau and part of Xinjiang Province (Fig. 6b). However, comparing to the projected changes in HWN, the projected changes of HWDU are less robust, with the ratios of changes to the intermodel spread generally within the range of 1.0–3.0 and less than 1.0 over the central eastern China. Regarding the HWM, the strongest increases of over 0.5°C/day are located in northeastern China, followed by the changes over southern China, the eastern Tibetan Plateau and northwestern China (Fig. 6c). The robustness of the projected changes of HWM is higher than those of HWDU but lower than those of HWN, with

the ratios to the intermodel spread over most of China higher than 1.0 but lower than 4.0. As the combination of HWDU and HWM, HWI shows the greatest increase above 4.0°C/event over northeastern China, southern China, and the eastern Tibetan Plateau (Fig. 6d). The ratios of changes to the intermodel spread is generally within the range of 1.0–4.0. HWF and HWTI would experience changes with similar patterns, demonstrating higher increases over the west and south parts of China that are very high robust, that the ratios to the intermodel spread are higher than 2.0 over most of China and higher than 5.0 over the northern China.

The above results cover the robustness or uncertainty in the future changes of heat waves projected by the model ensemble. It has been demonstrated that the projected changes in heat waves are qualified as robust over most of

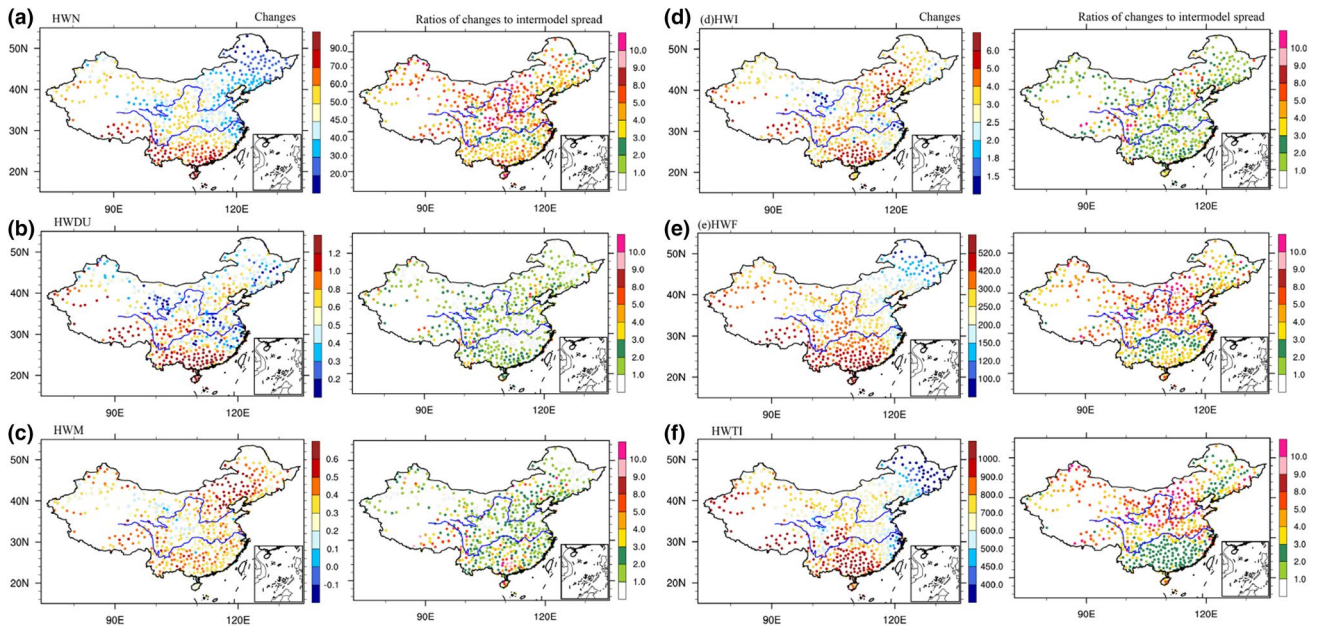


Fig. 6 The spatial distributions of the future changes in heat wave indices in the model ensemble (FTR-RF, left one in each panel) and the ratios of the future changes to the intermodel spread (right one in each panel) for HWN (a), HWDU (b), HWM (c), HWI (d), HWF (e), and HWTI (f)

China. In addition, the projected changes in the accumulated properties of heat waves, i.e., HWN, HWF and HWTI show higher robustness than those of HWDU, HWM and HWI, especially over the northern part of China.

Figure 7 shows the percentages of areas for heat wave indices with different values over the RF and FTR periods. The distinctions between heat wave characteristics in RF and FTR periods are obvious. For both the singular and

integrative heat wave indices, the future projected heat waves in the model ensemble show increases in their mean value and spatial variability, except for HWI (statistic values in Table 1). The four WRF simulations driven by different GCMs exhibit great consistency in the projections of heat wave changes (Fig. 7a–f), although with the existence of intermodel spread. The shift towards higher values and increased variabilities of heat wave indices indicate that

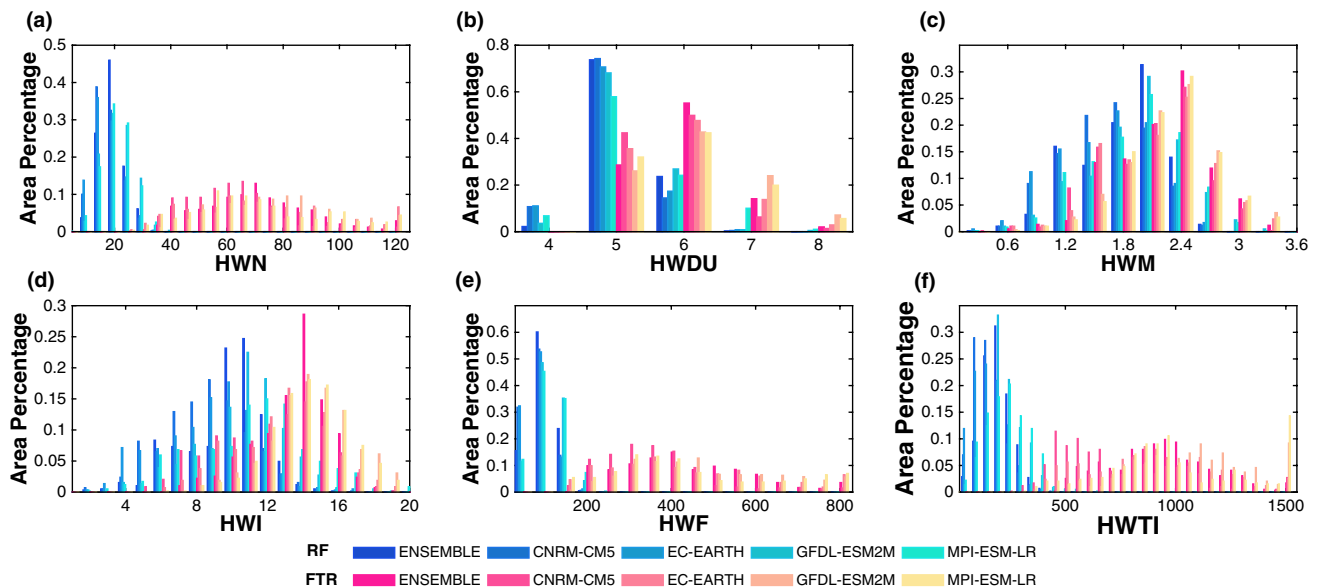


Fig. 7 The histograms of area percentages for HWN (a), HWDU (b), HWM (c), HWI (d), HWF (e) and HWTI (f) in the four WRF simulations driven by different GCMs and the model ensemble in the RF (1981–2005) and FTR (2031–2055) periods

Table 1 The mean and standard deviation (STD) for each heat wave index at the 587 observation sites in the model ensemble in the RF (1981–2005) and FTR (2031–2055) periods

	RF		RCP	
	Mean	STD	Mean	STD
HWN	19.87 (1.92)	4.33 (0.20)	70.3 (5.42)	20.57 (3.44)
HWDU	5.20 (0.15)	0.42 (0.12)	5.94 (0.18)	0.83 (0.16)
HWM	1.81 (0.15)	0.45 (0.02)	2.18 (0.09)	0.48 (0.02)
HWI	9.78 (1.16)	2.33 (0.37)	13.22 (1.02)	2.08 (0.28)
HWF	104.69 (12.91)	28.97 (3.08)	434.43 (46.35)	199.11 (32.29)
HWTI	197.45 (40.05)	66.10 (10.95)	922.40 (130.73)	232.70 (32.66)

The intermodel spread is given in the bracket. Unit: HWN (events), HWDU (days/event), HWM (°C/day/event), HWI (°C/event), HWF (days), and HWTI (°C)

more areas will be exposed to more frequent, prolonged, severe and intense heat waves in the coming decades. Moreover, the changes in heat waves are more obvious in terms of HWN, HWF and HWTI (Fig. 7a, e, f) as their values in RF and FTR rarely overlap, indicating that the impacts of climate changes on the accumulated properties of heat waves are more substantial. The very low values of the intermodel spread (Table 1, in the bracket) among the four WRF simulations are in agreement with the results in Fig. 6 and further confirm the robustness of heat wave changes projected by the model ensemble. Thus, the following analyses and discussions are mainly based on the ensemble results of four WRF simulations.

To understand the future changes in heat waves more precisely, the future changes projected by the model ensemble for the six heat wave indices are also expressed by a ratio $((FTR-RF)/RF)$, which is a representative of their sensitivity to climate changes and shown in Fig. 8. For the HWN, the ratios show higher values above 3.0 over Xinjiang, southern China and the middle to lower reaches of the Yellow River (Fig. 8a). The ratios of the changes in HWDU are generally lower than those for HWN, with values greater than 0.1 over most areas of China, except for parts of northeastern and southern China and the upper reaches of the Yellow River (Fig. 8b). The relative changes in HWM also have lower values than those of HWN, which are ranging from 0.1 to 0.5 over most areas of China, with the maximum values above 0.3 in the southern, eastern and the middle to lower reaches of the Yellow River (Fig. 8c). The HWI shows a similar spatial pattern of relative changes to that of HWM, with maximum values above 0.5 over the above-mentioned areas (Fig. 8d). The spatial patterns of relative changes in HWF and HWTI are similar to those of HWN but with even higher magnitude, which can reach 4 and 8, respectively (Fig. 8e, f). The results show that the changes in the accumulated properties of heat waves, i.e., the frequency, total days and total intensity, are more sensitive to climate changes than the mean duration, severity and intensity of heat waves. Consistent with the above analyses, the results highlight the considerable accumulated impacts of climate change on heat waves. Moreover, all six heat wave indices show higher change ratios over northwestern and southern China and the middle to lower reaches of the Yellow River, indicating that heat waves over these regions are more sensitive to the changing climate. These findings should raise

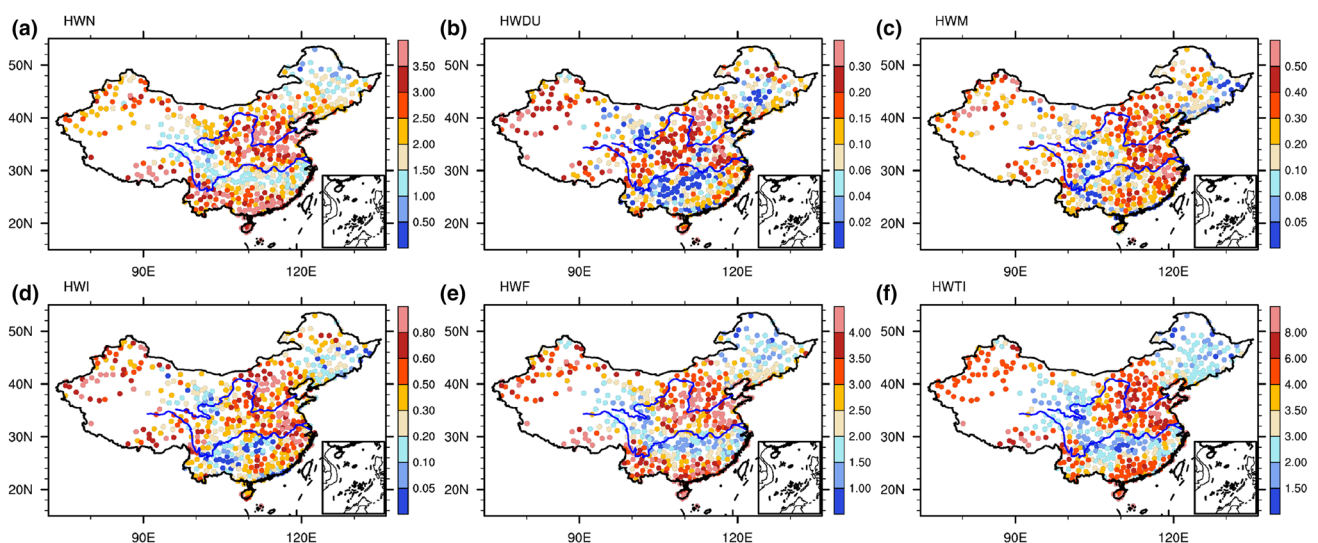


Fig. 8 The spatial distributions of future changes in a ratio $((FTR-RF)/RF)$ for HWN (a), HWDU (b), HWM (c), HWI (d), HWF (e), and HWTI (f)

awareness of the need for disaster preventions over these regions.

To investigate the changes in the interannual variability of heat waves, the interannual variations of heat wave indices in the model ensemble averaged over all of China during RF and FTR periods are shown in Fig. 9. For heat waves in the RF period, all the six indices show clear interannual variations and exhibit notable increasing trends, which are all significant at the 99% confidence level with the exceptions of HWM and HWI (Fig. 9c, d). The values of all six heat wave indices in the FTR period are obviously increased compared to those in the RF period, with the minimum values generally higher than the maximum values in the RF period. Moreover, all the six heat wave indices exhibit significant increasing trends in the FTR period and the trends are higher than those in the RF period, except for HWM (Fig. 9c), indicating a more rapid increase in heat wave indices in the future. The increasing trends of HWN, HWF and HWTI in the FTR period are more than 3 times of those in the RF period, which are much greater than the changes in the other heat wave indices. This is consistent with the above results shown in Figs. 7 and 8, suggesting that the climate changes impose more considerable impacts on the accumulated properties of heat waves.

3.3.2 Future changes in the probability of heat wave events

The above results investigate the changes in the climatology and interannual variability of the averaged heat wave indices. In this section, we focus on the changes in characteristics in the view of individual heat wave events (i.e.,

the duration, magnitude, and intensity during a heat wave event). Global warming is expected to increase the probability of warm temperature extremes. Understanding the probability distribution of future temperature extremes has important implications for human and ecosystem acclimation (Guirguis et al. 2018). The probability density functions (PDFs) of HWI, HWDU and HWM in the model ensemble for all the heat wave events in the RF (1981–2005) and FTR periods (2031–2055) are presented in Fig. 10. For HWI, the mean value in the FTR period is projected to be twice of that of the RF period, and it demonstrates a wider range of values with a significant increase in the standard deviation. Consequently, there is a notable change in the shape of the PDF, with the probability of weak heat waves with HWI values lower than 2.5 °C generally decreases, while the probability of stronger heat wave events increases in the future (Fig. 10a). Such changes are also prominent for the heat wave duration and magnitude, with significant increases in the mean values and standard deviations (Fig. 10b, c). The changes in the PDFs of HWI, HWDU and HWM indicate that stronger heat waves with prolonged duration and greater magnitude will occur more often in the FTR period, while weaker heat waves would occur less often and are shorter and more moderate on average. Additionally, the projected changes in the PDFs of heat wave events are consistent in the four WRF simulations (Fig. S9).

To specifically estimate the future changes in the occurrences of heat waves with different intensities, heat waves are classified into four categories by the HWI. The classification criteria are as follows: 0 °C < normal ≤ 4 °C < moderate ≤ 8 °C < severe ≤ 12 °C < extreme (Wang et al. 2018). It can be noticed in Fig. 10a that the probability of normal

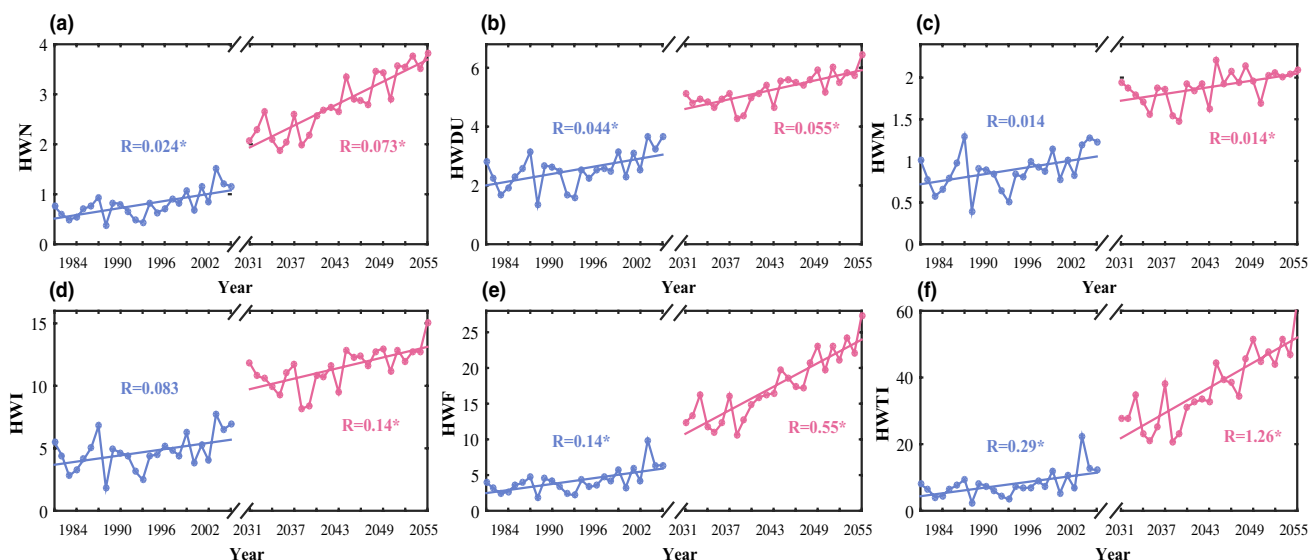


Fig. 9 The interannual variations of averaged heat wave indices across all of China during the RF and FTR periods. R values indicate the linear trend for the annual mean heat wave indices. The black star denotes the trends above the 99% confidence level

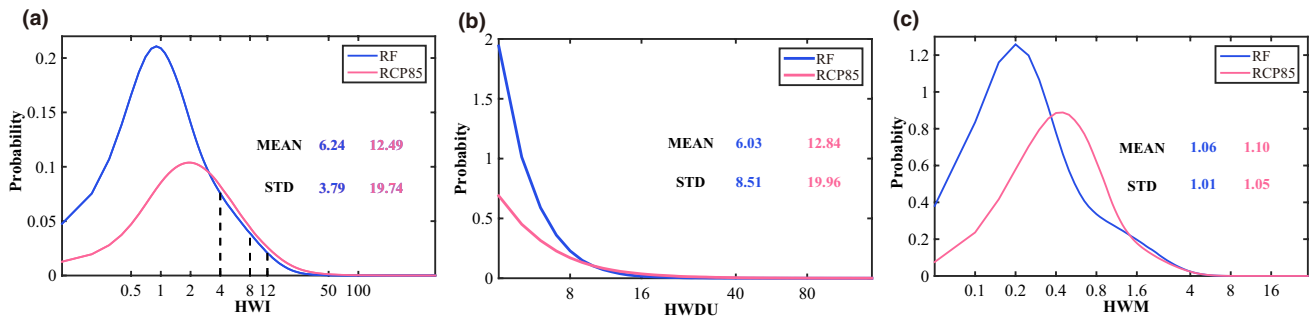


Fig. 10 The probability density functions (PDFs) of HWI, HWDU and HWM for all heat wave events in RF (1981–2005) and FTR periods (2031–2055)

heat waves is decreased while that of moderate to extreme heat waves is increased in the FTR period. Figure 11a shows the histograms of frequency changes (FTR-RF) for heat wave occurrences in the model ensemble in each category. The frequency is expressed as a percentage. It's shown that the frequency of normal heat waves is reduced in the FTR period, whereas the frequency of moderate to severe heat waves is increased, with the most obvious increase in the frequency of extreme heat waves. The spatial patterns of absolute changes in heat wave occurrences for different categories are shown in Fig. 11b–e. Consistent with results in Fig. 11a, among the four categories, the occurrence of extreme heat waves shows the most remarkable increase in the coming decades (Fig. 11e), followed by the moderate and severe heat waves (Fig. 11c, d), and the normal heat waves show the least increase (Fig. 11b). Moreover, for the extreme heat wave events, the strong increases dominate all of China (Fig. 11e), whereas the increases in normal to severe heat waves are relatively higher over southern China (Fig. 11b–d), which is consistent with the results in Fig. 6a. These results exhibit a challenging situation for human health and the environment in China, under which extremely high temperatures will be dramatically increased in the upcoming years, and more attention should be paid on the adaption strategies to address such crises. It should be noted that such changes in heat wave occurrences show great consistency among the four WRF simulations (Fig. S10–S11).

3.3.3 Future changes in the large-scale circulation

As discussed above, high-pressure systems are fundamental for sustaining heat waves. Considering the significant relationship between heat wave events and the synoptic circulation, it is reasonable to connect the changes in heat wave characteristics to the changes in the related synoptic circulation. First, we analyze the synoptic circulation during heat waves in the FTR period (2031–2055). Similar to

Fig. 5, the H500 anomalies in the model ensemble during heat waves at the three sites in the FTR period are shown in Fig. 12. Heat waves in different regions of China in future decades are also dominated by significant high-pressure systems (Fig. 12a–c). Herein, for each grid, we define that high-pressure system conditions occur when the daily H500 exceeds the average H500 during May to September over the reference period (1981–2005). Figure 13 shows the future changes (FTR-RF) in the total high-pressure system days (a), mean duration of high-pressure systems (b), and the mean magnitude of H500 anomalies during heat wave periods (c). The changes in the total days of high-pressure systems correspond well to the changes in HWN (Fig. 6a), with a spatial correlation above 0.7. The changes are distributed with a decreasing trend from south to northeast China, with higher changes located over southern China, dominating the higher increase of HWN (Fig. 13a). Moreover, the changes in the mean duration of high-pressure systems match the changes in the HWDU very well (Fig. 6b), with a significant spatial correlation of 0.39. The greatest changes in the mean duration of high-pressure systems co-occur with the highest increase of HWDU over southern China and with weaker changes in northeastern China (Fig. 13b). In addition, the changes in the mean values of H500 anomalies over heat wave periods show good agreement with the changes in HWM and HWI (Fig. 6c, d), presenting higher increases over southern China, the Tibetan Plateau and part of northeastern China (Fig. 13c), exhibiting a spatial correlation of 0.3 with the changes in HWI (Fig. 6d). It can be concluded that the increased frequency and duration of high-pressure systems in the future can reasonably account for the changes in the frequency and duration of heat waves. In addition, the changes in the magnitude of the high-pressure systems during heat waves can explain the changes of heat wave intensity to a great extent. In other word, the changes in the characteristics of heat waves are closely related to the changes in the dominance of high-pressure systems.

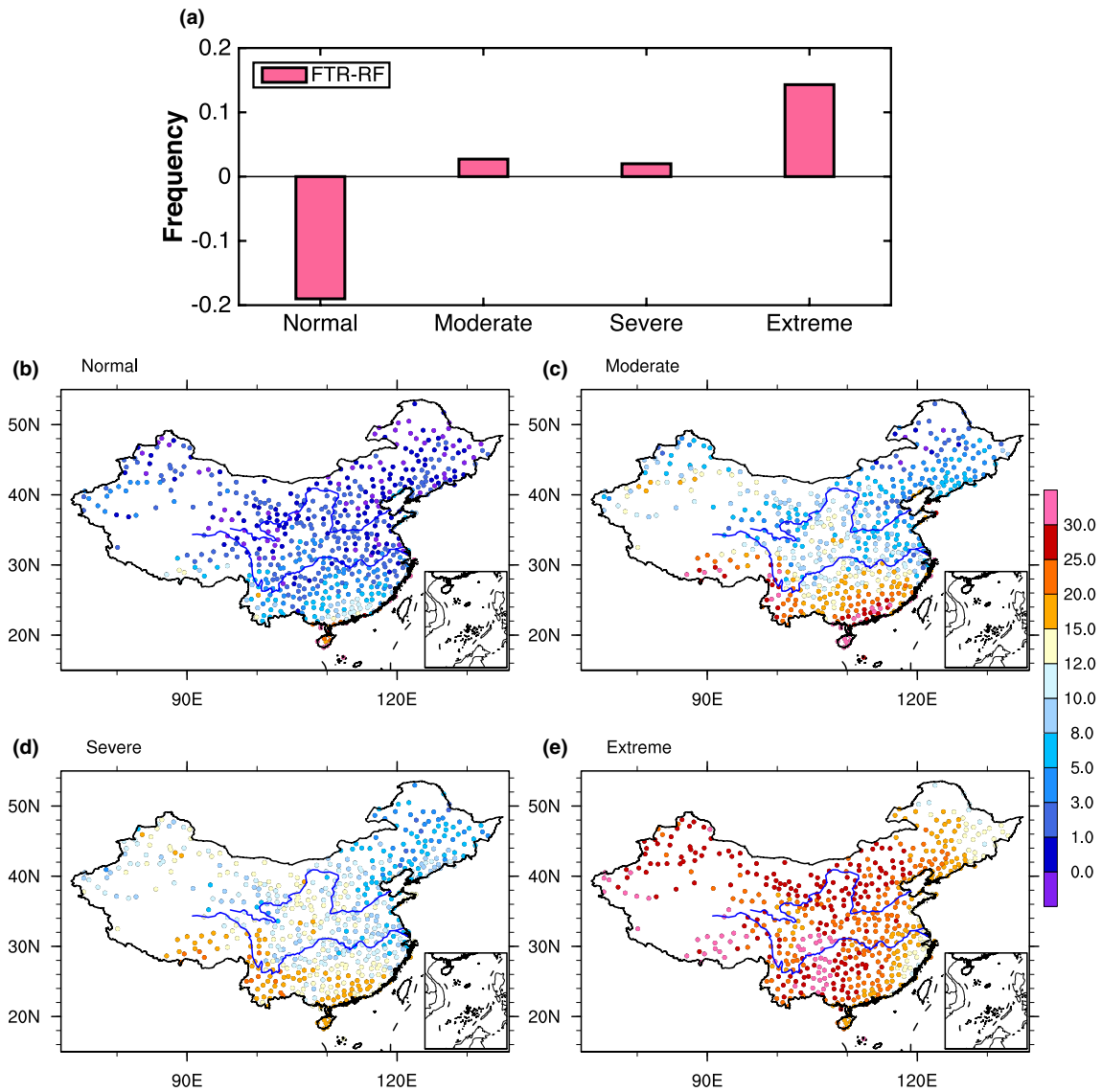


Fig. 11 The projected changes in the frequency of heat wave occurrences in different categories in the model ensemble (a) and the spatial distributions of the projected changes in the occurrences of normal (b), moderate (c), severe (d) and extreme heat waves (e)

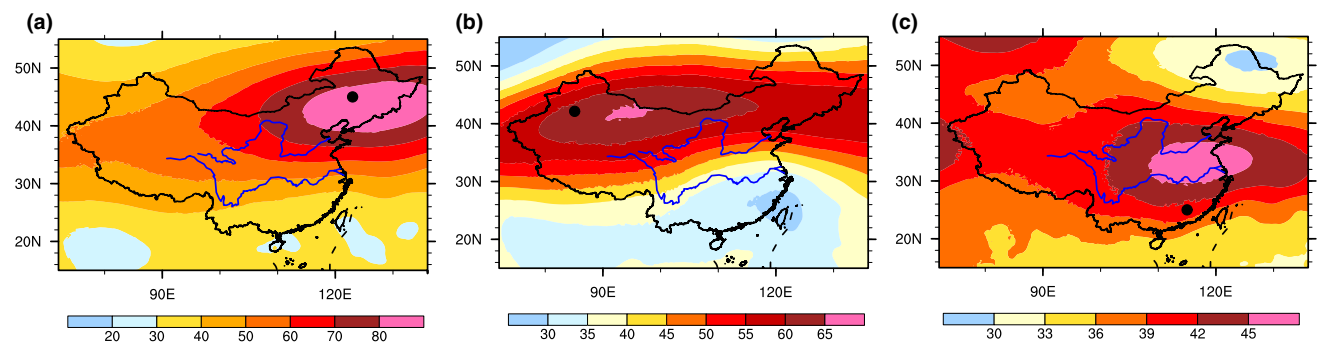


Fig. 12 Same as Fig. 5, but for the H500 anomalies (unit: m) during heat waves at eastern (45°N, 123°E), northwestern (42°N, 85°E) and south-eastern China (25°N, 115°E) in the FTR period

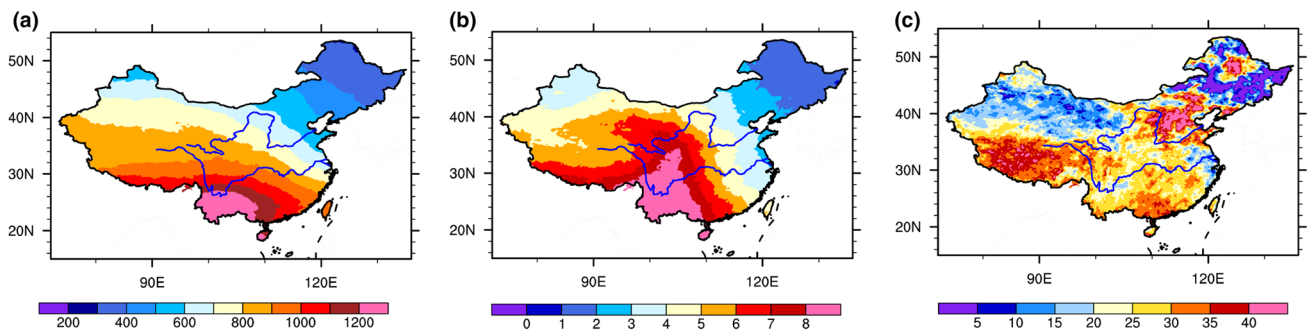


Fig. 13 The future changes (FTR-RF) in the total high-pressure system days **(a)**, unit: days), mean duration of high-pressure systems **(b)**, unit: days) and the mean H500 anomalies during heat wave periods

(c), unit: m). The high pressure means the daily H500 value exceeding the mean H500 during May to September for 1981–2005

4 Conclusions

In this study, the future changes in heat waves over China are investigated by the WRF model under the warming scenario RCP8.5, with the aim of supporting policy making and strategy adaptations for China and motivating to call for more public attention on climate change and its consequences. The initial and boundary conditions in the WRF simulations are provided by four GCMs from CMIP5 (i.e., CNRM-CM5, EC-EARTH, GFDL-ESM2M and MPI-ESM-LR). The simulations include historical runs under present climate condition (1981–2005), which is defined as the reference period (RF), and the future projection (2031–2055, FTR). Heat waves in historical runs and future projections are both defined based on present-day standards. Six heat wave indices, including singular and integrative indices (i.e., HWN, HWDU, HWM, HWI, HWF and HWTI) are used to measure different aspects of heat wave characteristics.

We first evaluate the ability of the WRF model to reproduce the heat waves in the present climate. The results show that the model runs driven by the four GCMs can reproduce the spatial patterns of all heat wave indices in the present climate reasonably well, although differences exist among the four simulations. Moreover, the ensemble of the four model experiments generally shows a better presentation for the spatial pattern and magnitude of heat wave indices, with higher spatial correlation and lower biases. Heat waves are generally dominated by regionally anomalous high-pressure systems. The WRF model shows the capability to correctly capture the spatial location and magnitude of the synoptic circulation that dominates heat waves.

The spatial distributions of changes in heat wave indices (FTR-RF) show that increased changes in all heat wave indices cover almost all of China. Moreover, the histograms of the percentages of areas for heat wave indices with different values exhibit a shift towards increased mean value and variability, indicating that more areas will experience more frequent, longer lasting, more severe heat waves in the

coming decades. To further investigate the sensitivity of heat waves to climate changes, the future changes of the six heat wave indices are also expressed as ratios ((FTR-RF)/RF). Results show that all the six heat wave indices show higher change ratios over northwestern and southern China as well as the middle to lower reaches of the Yellow River, indicating that heat waves over these regions are more sensitive to the changing climate. The impacts of climate changes on the accumulated properties of heat waves (i.e., HWN, HWF and HWI) are more substantial than the singular indices, i.e., HWDU, HWM and HWI. The projected interannual variations of the six heat wave indices exhibit notable increasing trends, which are more significant than those in the RF period, indicating that the heat waves will intensify more rapidly in the future.

We further focus on the changes in the characteristics of individual heat wave events by analyzing the changes in the PDFs of HWDU, HWM, and HWI. The results indicate that stronger heat waves with longer durations and stronger intensities will occur more often in the FTR period, while weaker heat waves will occur less often. By quantitatively classifying heat waves into four categories based on their intensities, namely, normal, moderate, severe and extreme heat waves, it is shown that the frequency of normal heat waves is reduced in the FTR period, whereas the frequency of moderate to severe heat waves is increased, especially the frequency of extreme heat waves. It is also noted that southern China is expected to face greater risk from the increased heat waves. More attention should be paid to the adaptation strategies to address such crises.

The changes in the characteristics of heat waves can be attributed to the changes in the synoptic circulation. It is indicated that the changes in the total days and mean duration of the high-pressure systems correspond well to the changes in the heat wave frequency and mean duration. In addition, the changes in the magnitude of H500 anomalies during heat waves can explain the changes of heat wave intensity to a great extent.

Additionally, it should be noted that, although there are intermodel differences, the projected changes in heat waves are largely consistent among the four WRF simulations driven by different GCMs, especially for the accumulated properties of heat waves.

Acknowledgements This work is supported by the National Key R&D Program of China (2018YFA0606003) and the National Natural Science Foundation of China (91425304, 41575099 and 41375075). The authors also acknowledge with thanks the GFDL, CNRM and MPI organizations for providing the CMIP5 data as the driving fields in the WRF simulations, as well as the ICTP for providing the EC-EARTH data.

Compliance with ethical standards

Conflict of interest We declare that we have no conflict of interest.

References

- Barriopedro D, Fischer EM, Luterbacher J, Trigo RM, García-Herrera R (2011) The hot summer of 2010: redrawing the temperature record map of Europe. *Science* 332(6026):220–224
- Beniston M, Stephenson DB, Christensen OB, Ferro CAT, Frei C, Goyette S, Halsnaes K, Holt T, Jylhä K, Koffi B (2007) Future extreme events in European climate: an exploration of regional climate model projections. *Clim Change* 81(1):71–95
- Boo KO, Kwon WT, Baek HJ (2006) Change of extreme events of temperature and precipitation over Korea using regional projection of future climate change. *Geophys Res Lett* 33(1):313–324
- Bosmans J, Erb MP, Dolan AM et al (2018) Response of the Asian summer monsoons to idealized precession and obliquity forcing in a set of GCMs. *Quat Sci Rev* 188:121–135
- Chen F, Dudhia J (2001) Coupling an advanced land surface hydrology model with the Penn State-NCAR MM5 modeling system Part I: model implementation and sensitivity. *Mon Weather Rev* 129(4):569–585
- Chen H, Sun J (2013) Projected change in East Asian summer monsoon precipitation under RCP scenario. *Meteorol Atmos Phys* 121(1–2):55–77
- Cowan T, Purich A, Perkins S, Pezza A, Bosch G, Sadler K (2014) More frequent, longer, and hotter heat waves for Australia in the twenty-first century. *J Clim* 27(15):5851–5871. <https://doi.org/10.1175/JCLI-D-14-00092.1>
- Ding T et al (2010) Changes in hot days and heat waves in China during 1961–2007. *Int J Climatol* 30(10):1452–1462
- Dosio A (2016) Projection of temperature and heat waves for Africa with an ensemble of CORDEX Regional Climate Models. *Clim Dyn* 49:1–27
- Dosio A, Panitz HJ, Schubert-Frisius M et al (2015) Dynamical downscaling of CMIP5 global circulation models over CORDEX-Africa with COSMO-CLM: evaluation over the present climate and analysis of the added value. *Clim Dyn* (2015) 44:2637. <https://doi.org/10.1007/s00382-014-2262-x>
- Dosio A, Mentaschi L, Fischer EM, Wyser K (2018) Extreme heat waves under 1.5 °C and 2 °C global warming. *Environ Res Lett*. <https://doi.org/10.1088/1748-9326/aab827>
- Ebita A, Kobayashi S, Ota Y, Moriya M, Kumabe R, Onogi K et al (2011) The Japanese 55-year reanalysis “JRA-55”: an interim report. *Sci Online Lett Atmos Sola* 7(1):149–152
- Field CB, Barros V, Stocker TF, Dahe Q, Dokken DJ, Ebi KL, Mastrandrea MD, Mach KJ, Plattner GK, Allen SK (2012) Managing the risks of extreme events and disasters to advance climate change adaptation. Special report of the Intergovernmental Panel on Climate Change (IPCC). *J Clin Endocrinol Metab* 18(6):586–599
- Fischer EM, Seneviratne SI, Vidale PL, Lüthi D, Schär C (2007) Soil moisture atmosphere interactions during the 2003 European summer heat wave. *J Clim* 20(20):5081
- Giorgi F, Gutowski J (2015) Regional Dynamical Downscaling and the CORDEX Initiative. *Annu Rev Environ Resour* 40(1):150724171620008
- Giorgi F, Jones C, Asrar G (2009) Addressing climate information needs at the regional level: the CORDEX framework. *Organization (WMO). Bulletin* 58:175–183
- Griffiths GM et al (2005) Change in mean temperature as a predictor of extreme temperature change in the Asia-Pacific region. *Int J Climatol* 25:1301–1330
- Guirguis K, Gershunov A, Cayan DR, Pierce DW (2018) Heat wave probability in the changing climate of the Southwest US. *Clim Dyn* 50(9–10):3853–3864
- Guo X, Huang J, Luo Y, Zhao Z, Xu Y (2016) Projection of heat waves over China for eight different global warming targets using 12 CMIP5 models. *Theor Appl Climatol* 128:1–16
- Hong SY, Noh Y, Dudhia J (2006) A new vertical diffusion package with an explicit treatment of entrainment processes. *Mon Weather Rev* 134:2318–2341
- Hudson D, Marshall AG, Alves O (2011) Intraseasonal forecasting of the 2009 summer and winter Australian heat waves using POAMA. *Weather Forecast* 26(3):257–279
- IPCC (2014) Climate Change 2014: synthesis report. Contribution of working groups I, II and III to the fifth assessment report of the intergovernmental panel on climate change [Core Writing Team, Pachauri RK, Meyer LA (eds)], IPCC, Geneva, Switzerland, pp 151
- Kain JS, Fritsch JM (1990) A one-dimensional entraining/detraining plume model and its application in convective parameterization. *J Atmos Sci* 47:2784–2802
- Kunkel KE, Liang XZ, Zhu JH (2010) Regional climate model projections and uncertainties of U.S. summer heat waves. *J Clim* 23(23):4447–4458
- Lhotka O, Kyselý J (2015) Spatial and temporal characteristics of heat waves over Central Europe in an ensemble of regional climate model simulations. *Clim Dyn* 45(9–10):2351–2366
- Li B, Zhou T (2010) Projected climate change over China under SRES A1B scenario: multi-model ensemble and uncertainties. *Clim Change Res* 6(04):270–276
- Li Q, Liu X, Zhang H, Peterson TC, Easterling DR (2004) Detecting and adjusting temporal in-homogeneity in Chinese mean surface air temperature data. *Adv Atmos Sci* 21(2):260–268
- Lim KSS, Hong SY (2010) Development of an effective double-moment cloud microphysics scheme with prognostic cloud condensation nuclei (CCN) for weather and climate models. *Mon Weather Rev* 138:1587–1612
- Lu R, Chen D (2016) A review of recent studies on extreme heat in China. *Atmos Ocean Sci Lett* 9(2):114–121
- Matsueda M (2011) Predictability of Euro-Russian blocking in summer of 2010. *Geophys Res Lett* 38(6):122–133
- Meehl GA, Tebaldi C (2004) More intense, more frequent, and longer lasting heat waves in the 21st century. *Science* 305(305):994–997
- Meehl GA et al (2000) An introduction to trends in extreme weather and climate events: observations, socioeconomic impacts, terrestrial ecological impacts, and model projections. *Bull Am Meteorol Soc* 81:413–416
- Orlowsky B, Seneviratne SI (2011) Global changes in extreme events: regional and seasonal dimension. *Clim Change* 110(3–4):669–696. <https://doi.org/10.1007/s10584-011-0122-9>

- Perkins SE (2015) A review on the scientific understanding of heat waves—their measurement, driving mechanisms, and changes at the global scale. *Atmos Res* 164:242–267
- Pezza AB, Rensch PV, Cai W (2012) Severe heat waves in Southern Australia: synoptic climatology and large scale connections. *Clim Dyn* 38(1):209–224
- Russo S, Sterl A (2011) Global changes in indices describing moderate temperature extremes from the daily output of a climate model. *J Geophys Res* 116(D3):D03,104. <https://doi.org/10.1029/2010JD014727>
- Sillmann J, Kharin VV, Zwiers FW, Zhang X, Bronaugh D (2013) Climate extremes indices in the CMIP5 multimodel ensemble: part 2. Future climate projections. *J Geophys Res Atmos* 118(6):2473–2493. <https://doi.org/10.1002/jgrd.50188>
- Skamarock WC, Klemp JB, Dudhia J, Gill DO, Barker DM, Duda MG, Huang X-Y, Wang W, Powers JG (2008) A description of the advanced research WRF version 3. NCAR technical note NCAR/TN-475 + STR, National Center for Atmospheric Research, Boulder
- Stefanon M, Fabio D, Drobinski P (2012) Heatwave classification over Europe and the Mediterranean region. *Environ Res Lett* 7(1):014023
- Tang J, Wang S, Niu X, Hui P, Zong P, Wang X (2016) Impact of spectral nudging on regional climate simulation over CORDEX East Asia using WRF. *Clim Dyn* 48:1–19
- Taylor KE (2001) Summarizing multiple aspects of model performance in a single diagram. *J Geophys Res Atmos* 106(D7):7183–7192
- Taylor KE, Stouffer RJ, Meehl GA (2012) An overview of CMIP5 and the experiment design. *Bull Am Meteor Soc* 93(4):485–498
- Tebaldi C, Hayhoe K, Arblaster JM, Meehl GA (2006) Going to the extremes. *Clim Change* 79(3–4):185–211. <https://doi.org/10.1007/s10584-006-9051-4>
- Unal YS, Tan E, Montes SS (2013) Summer heat waves over western Turkey between 1965 and 2006. *Theor Appl Climatol* 112(1–2):339–350
- Wang W, Zhou W, Li Y, Wang X, Wang D (2015) Statistical modeling and CMIP5 simulations of hot spell changes in China. *Clim Dyn* 44(9–10):2859–2872
- Wang P, Tang J, Wang S, Dong X, Fang J (2017a) Regional heatwaves in china: a cluster analysis. *Clim Dyn* 50:1–17
- Wang P, Tang J, Sun X, Wang S, Wu J, Dong X, Fang J (2017b) Heatwaves in China: definitions, leading patterns and connections to large-scale atmospheric circulation and SSTs. *J Geophys Res Atmos* 122:20
- Wang P, Tang J, Sun X, Liu J, Fang J (2018) Spatiotemporal characteristics of heat waves over China in regional climate simulations within the CORDEX-EA project. *Clim Dyn* 8:1–20
- Yang H, Xu Y, Zhang L, Pan J, Li X (2010) Projected change in heat waves over China using the PRECIS climate model. *Clim Res* 42(1):79–88
- Yao Y, Luo Y (2012) Evaluation and projection of temperature extremes over China based on 8 modeling data from CMIP5. *Progressus Inquisitiones De Mutatione Climatis* 8:250–256
- Zhang Y (2012) Projections of 2.0 °C warming over the globe and China under RCP4.5. *Atmos Ocean Sci Lett* 5(6):514–520
- Zhou W, Tang J, Wang X, Wang S, Niu X, Wang Y (2016) Evaluation of regional climate simulations over the CORDEX-EA-II domain using the COSMO-CLM model. *Asia Pac J Atmos Sci* 52(2):107–127
- Zittis G, Hadjinicolaou P, Fnais M, Lelieveld J (2016) Projected changes in heat wave characteristics in the eastern Mediterranean and the Middle East. *Reg Environ Change* 16:1–14

Publisher's Note Springer Nature remains neutral with regard to jurisdictional claims in published maps and institutional affiliations.